



Universiteit
Leiden
The Netherlands

A photo-switchable peptide fibril esterase

Samanta, M.; Saad, N.; Wu, D.; Crone, N.S.A.; Abramov-Harpaz, K.; Regev, C.; ... ; Ashkenasy, G.

Citation

Samanta, M., Saad, N., Wu, D., Crone, N. S. A., Abramov-Harpaz, K., Regev, C., ...
Ashkenasy, G. (2024). A photo-switchable peptide fibril esterase. *Angewandte Chemie
(International Edition)*, 64(1). doi:10.1002/anie.202413810

Version: Publisher's Version

License: [Creative Commons CC BY 4.0 license](#)

Downloaded from: <https://hdl.handle.net/1887/4176774>

Note: To cite this publication please use the final published version (if applicable).

Peptide Catalysis

A Photo-Switchable Peptide Fibril Esterase

Mousumi Samanta⁺, Noy Saad⁺, Dinghao Wu⁺, Niek S. A. Crone⁺, Karina Abramov-Harpaz, Clil Regev, Rivka Cohen-Luria, Aimee L. Boyle, Yifat Miller,^{*} Alexander Kros,^{*} and Gonen Ashkenasy^{*}

Abstract: Recent attempts to mimic enzyme catalysis using simple, short peptides have been successful in enhancing various reactions, but the on-demand, temporal or spatial regulation of such processes by external triggers remains a great challenge. Light irradiation is an ideal trigger for regulating molecular functionality, since it can be precisely manipulated in time and space, and because most reaction mediums do not react to light. We herein report the selection of a photo-switchable amphiphilic peptide catalyst from a small library of isomeric peptides, each containing an azobenzene-based light responsive group and a catalytic histidine residue. In its native fibrillar form, the selected peptide is efficiently and enantio-selectively active for ester hydrolysis, but after irradiation by UV light inducing *trans*-to-*cis* azobenzene isomerization, the fibrils disassemble to amorphous aggregates that are much less catalytically active. Significantly, this esterase-like activity can be manipulated multiple times, as the fibrillar peptide assembly is reversibly reduced and restored upon alternate irradiation by UV and visible light, respectively. We propose that this research may shine light on the origin of complex functions in early chemical evolution. Furthermore, it paves the way to regulate additional functions for peptide nanotechnology, such as replication, charge transfer, and delivery.

Introduction

Extremely efficient and specific enzyme catalysis evolved over billions of years when polypeptide sequences have been synthesized, duplicated or modified, until their 3D structures and folding dynamics were perfected to bind their respective substrates and release the products. In current biology, the regulation of enzymatic activity is pivotal for a range of processes during the cell cycle, including metabolism, signal transduction, differentiation, and cell growth. Such regulation is achieved by a molecular response to physicochemical cues, such as light irradiation, changes in temperature or pH, or binding ions and cofactor molecules.

Ongoing research in biomimetic systems chemistry targets similar evolutionary processes in which simple molecules—presumably peptides—emerge in the environ-

ment, combine, or gradually altered and transformed to acquire structure and (catalytic) activity.^[1] Accordingly, numerous studies reported on the propensity of short peptides to assemble into elongated structures, mostly fibres, and catalyse chemical transformations.^[2] Yet, temporal or spatial regulation of the structure and function of such assemblies by external triggering remains a great challenge. We herein describe a two-step selection process for discovering a photo-sensitive amphiphilic sequence in a small library of peptides, each containing an azobenzene-based light responsive side chain and a catalytic histidine residue (Scheme 1). This photo-switchable peptide undergoes multiple assembly-disassembly cycles in response to alternating UV and visible light irradiation, which in-turn halt (off) or restore (on) the stereo-selective hydrolysis of ester substrates.

[*] Dr. M. Samanta,⁺ N. Saad,⁺ K. Abramov-Harpaz, Dr. C. Regev, Dr. R. Cohen-Luria, Prof. Y. Miller, Prof. G. Ashkenasy
 Chemistry Department
 Ben-Gurion University of the Negev
 Campus st. 1, Beer Sheva, 8410501, Israel
 E-mail: ymiller@bgu.ac.il
 gonenash@bgu.ac.il

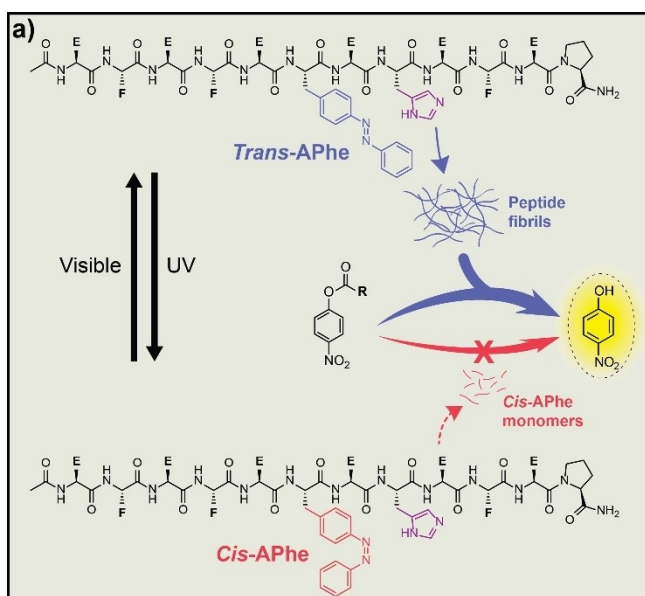
Dr. M. Samanta⁺
 Current address: Department of Chemistry
 Indian Institute of Technology
 New Delhi, 110016, India

D. Wu,⁺ Dr. N. S. A. Crone,⁺ Prof. A. Kros
 Supramolecular & Biomaterials Chemistry, Leiden Institute of Chemistry
 Leiden University
 2333CC, Leiden, The Netherlands
 E-mail: a.kros@chem.leidenuniv.nl

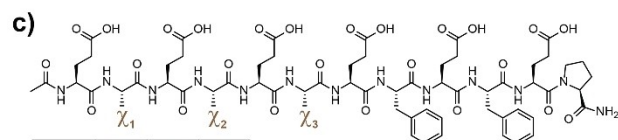
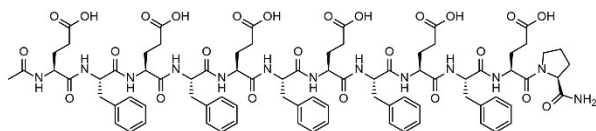
Dr. A. L. Boyle
 Macromolecular Biochemistry, Leiden Institute of Chemistry
 Leiden University
 2333CC, Leiden, The Netherlands
 Dr. A. L. Boyle
 Current address: School of Chemistry
 University of Bristol
 Cantock's Close, Bristol, BS8 1TS, UK

[†] These authors contributed equally to the paper.

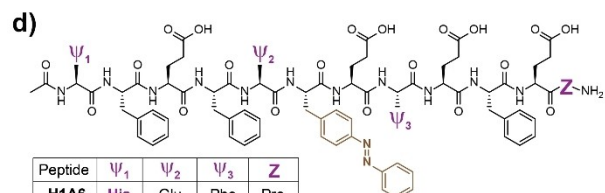
© 2024 The Authors. Angewandte Chemie International Edition published by Wiley-VCH GmbH. This is an open access article under the terms of the Creative Commons Attribution License, which permits use, distribution and reproduction in any medium, provided the original work is properly cited.



b) Primary amphiphilic sequence ('base' peptide)



Peptide	χ_1	χ_2	χ_3
A2	APhe	Phe	Phe
A4	Phe	APhe	Phe
A6	Phe	Phe	APhe



Peptide	ψ_1	ψ_2	ψ_3	Z
H1A6	His	Glu	Phe	Pro
H5A6	Glu	His	Phe	Pro
A6H8	Glu	Glu	His	Pro
A6H12	Glu	Glu	Phe	His

Scheme 1. The photo-switchable esterase system. **(a)** Reaction scheme. The initially assembled fibrils of the *trans*-APhe peptides are catalytically active. Shining UV light facilitates isomerization to the *cis*-APhe, and disassembles the supramolecular structures, practically abolishing the catalytic activity. The reverse *cis*-to-*trans* APhe isomerization by visible light readily affords reassembly and catalyst reactivation. **(b)** The basic peptide sequence used for designing the photo-switchable peptides.^[11c] **(c, d)** Chemical structures and nomenclature of the APhe peptides used for the investigation of photo-switched self-assembly studies (c), and combined photo-switched self-assembly and catalysis studies (d). Peptides synthesis and characterization are described in Supporting Information Scheme S1 and Figures S1–S2.

Biomimetic peptide fibril catalysts can accelerate different reactions in aqueous environments, including bond breaking (e.g., hydrolysis), aldol-type C–C bond formation,

oxidation reactions, and more.^[2a–c] The most efficient assemblies achieve strong catalytic activity, comparable (by weight) to those found in natural enzymes.^[3] Remarkably, only a handful of these systems present noticeable regio- or stereo-selectivity.^[4] A pioneering effort to regulate the catalytic activity of amphiphilic peptides applied pH jumps that induced the transition from an inactive random-coil peptide into a β -turn architecture, which in-turn assembled to fibres and enhanced ester hydrolysis.^[5] Recently, reciprocal enzymatic reactions were used to interconvert catecholase-mimicking peptides between active fibre assemblies and inactive amorphous particles.^[6] After several studies highlighted the spatiotemporal regulation of native protein functions by light,^[7] scientists have also used light irradiation to manipulate the structure and catalytic activity of supramolecular assemblies.^[8] Very recently, Das and co-workers have shown that short peptide assemblies can bind photosensitive cofactors and modulate aldolase-like activity. In their system, the catalytically more competent state was accessed by continuously shining light with high-energy photons.^[9]

Here, we present an alternative strategy for regulating peptide activity via incorporating, within a single sequence, both a photo-switchable group that reversibly facilitates the fibre assembly-disassembly process, and a catalytic group that promotes ester hydrolysis (Scheme 1a). The selected photo-switchable peptide possessed the azobenzene unit in the middle of the sequence, at the hydrophobic face together with His and Phe residues (Scheme 1a). Structure characterization assays revealed that this peptide gains a one order of magnitude higher propensity to assemble when the azobenzene side chain is in the *trans* configuration versus the *cis* configuration. Extensive molecular dynamics simulations highlighted the origin of the different assemblies for the two states, attributing it mainly to considerably strong interlayer π - π interactions between *trans*-azobenzene units, which were inaccessible to the tilted *cis*-azobenzene units. Consequently, ester hydrolysis rates were enhanced by ca. 40 times (versus background hydrolysis) by the *trans*-azobenzene peptide, about two times the rate enhancement observed for the *cis*-azobenzene peptide. The photo-switchable peptide was furthermore found to be enantioselective, displaying significant excess activity towards an *L*-amino acid ester versus a *D*-amino acid ester. Importantly, the above-mentioned structure and activity properties could be actively switched back-and-forth multiple times leading to disassembly and deactivation by UV light, and reassembly and reactivation by visible light.

Results and Discussion

Molecular Design of Light-Activated Peptide Catalysts

The photo-switchable peptide sequences were derived from the alternating “Glu-Phe” twelve *L*-amino acids sequence of a ‘base’ peptide (Scheme 1b). The short sequence, and the fact that the peptide sequence comprises only two types of amino acids, namely a minimal amino acids alphabet,

potentially supports its relevance to early chemical evolution in the prebiotic environment.^[1a,10] Like other peptides comprising of repetitive dyads of hydrophilic and hydrophobic amino acid residues, the base peptide can readily assemble into bilayer fibrillar architectures, in which the Phe residues form the hydrophobic core, and the glutamate side chains are pointing out to the aqueous environment. It was further revealed that the terminal proline residue can be used to enhance the formation of ordered β -sheet assemblies.^[11] We have previously shown that sequence modification via the integration of catalytic and auxiliary groups yields new derivatives that facilitate electron transfer along the main fiber axis,^[12] or catalyze aldol condensation,^[13] native chemical ligation and self-replication reactions.^[11d,14]

Here, in order to regulate the assembly propensity of amphiphilic peptides by light, we modified the basic peptide sequence by incorporating the light switchable phenylalanine-4-azobenzene ('Azo-phenylalanine'; APhe) residue into the 2nd, 4th, or 6th positions of the fiber hydrophobic core^[11c] (peptides **A2**, **A4**, **A6**; APhe represented by χ_1 - χ_3 in

Scheme 1c). Azobenzene derivatives have been frequently employed for fast back-and-forth switching of molecular structures—including peptide assemblies—and to induce changes in molecular function.^[15] For example, we have recently demonstrated that incorporating APhe residues into coiled-coil peptides can facilitate changes in peptide folding via UV light irradiation.^[16]

The presence of catalytic histidine residues at the active sites of many hydrolytic enzymes inspired their incorporation into prebiotically relevant peptide catalysts.^[2a,17] Consequently, after initial structural characterization of **A2**, **A4**, and **A6** peptides, which showed the highest effect of the azobenzene isomerization on the assembly of **A6** (see below; Figure 1a), we synthesized four derivatives of **A6** as organo-catalysts containing His moieties at different positions: a solvent-exposed position (**H5A6**), within the hydrophobic core (**A6H8**), at the N-terminus (**H1A6**), or C-terminus (**A6H12**) of the sequence (ψ_1 - ψ_3 positions in Scheme 1d). Characterization of this small peptide library would allow us to study the effect of light irradiation and consequent APhe

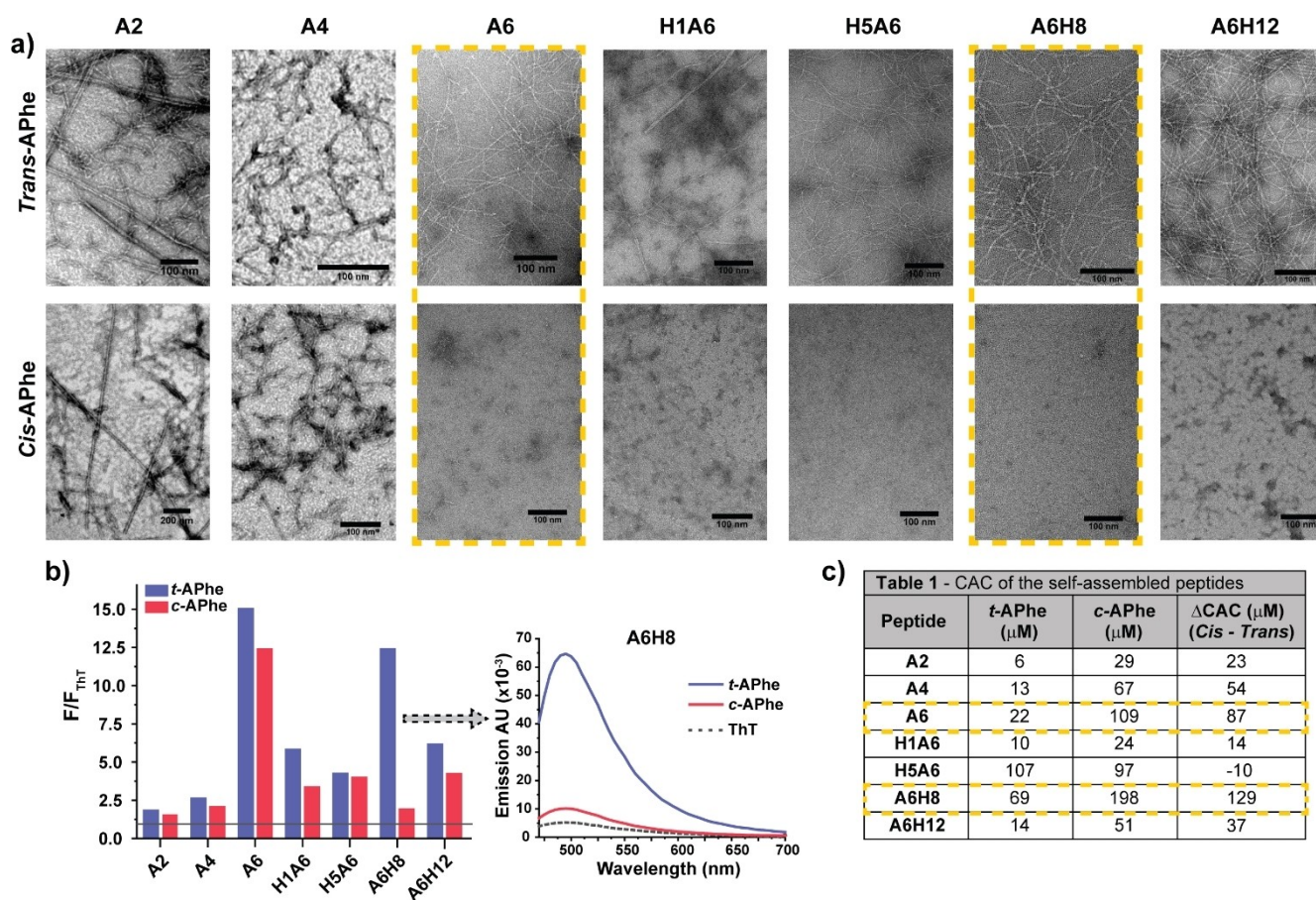


Figure 1. Self-assembly of amphiphilic β -sheet peptides possessing *trans*-APhe or *cis*-APhe residues. **(a)** TEM images of (200 μM) peptides containing the *t*-APhe (*top*) and *c*-APhe (*bottom*) isomers. Samples were stained with uranyl acetate before imaging. **(b)** ThT staining of (200 μM) peptides containing the *t*-APhe and *c*-APhe isomers. Fluorescence emission data at 500 nm (excitation at 440 nm) was normalized for emission of the ThT solution. Original emission spectra are shown in the graph on the right for **A6H8**, and in Figure S6 for all other peptides. Experiments were performed with 100 μM ThT in phosphate buffer pH 6.0 at 25 $^{\circ}\text{C}$. **(c)** Critical aggregation concentration (CAC) values determined from the light scattering plots (Figure S7).

isomerization on the peptide assembly and derived catalytic function.

Peptide Fibril Self-Assembly Regulated by Light

The effect of UV light illumination on the self-assembly propensity of **A2**, **A4**, and the five **A6**-derived peptides was investigated using various complementary tools (Figure 1). In a typical assay, the stock solution of the studied *trans*-APhe (*t*-APhe) peptide was prepared and either diluted into the buffer for structural characterization, or first illuminated (340–360 nm; 10–45 min, depending on the assay; see Supporting Information Experimental Methods (h)) to drive *trans*-to-*cis* isomerization and then diluted and investigated. From UV/Vis absorbance characterization, the level of *trans*-to-*cis* isomerization was found to be very similar for all peptides (Figure S4). For all peptides, transmission electron microscopy (TEM) images revealed the formation of fibrillar structures for the *t*-APhe peptides, and amorphous, or partially assembled aggregates for the corresponding *cis*-APhe (*c*-APhe) peptides (Figure 1a and Figure S5). The most significant differences in assembly morphology between the two states were observed for **A6** and **A6H8** (framed in yellow in Figure 1a). Thioflavin-T (ThT) staining assays, a typical indicator for the formation of β -sheet fibrillar structures, showed increased 500 nm fluorescence emission for the *t*-APhe peptides, versus the respective *c*-APhe peptides (Figure 1b). The largest difference was observed for **A6H8** with an almost 10-fold decrease in emission after *trans*-to-*cis* isomerization. The critical aggregation concentrations (CAC) of the *t*-APhe and *c*-APhe peptides (at fixed salt concentrations) were determined via light scattering. In all cases, except for **H5A6**, lower CAC values were obtained for the *t*-APhe versus the *c*-APhe peptides, indicating the tendency of the former to better aggregate (Figure 1c and Figure S7). Here again, the largest difference (Δ CAC) was observed for peptides **A6** and **A6H8**. Overall, the TEM, ThT assays and CAC measurements reveal that peptides **A6** and **A6H8** show the largest differences in assembly between the *t*-APhe and *c*-APhe forms, making these peptides the most suitable for further studies.

Characterization by circular dichroism (CD; Figure S8) revealed the formation of β -sheet architectures for the *t*-APhe **A6** and *t*-APhe **A6H8** assemblies, displaying a clear minimum at 214 nm, like the base peptide spectrum. After UV light illumination, the CD spectra of *c*-APhe peptides accounted for less defined structures with positive cotton effect peaks at \sim 220 nm. To gain a better understanding of the distinction between the peptide assemblies in the dark and after shining UV light, all-atom explicit molecular dynamics (MD) simulations were performed on two computationally constructed models of **A6H8**—**M1** and **M2**, representing the peptide assemblies of *t*-APhe **A6H8** and *c*-APhe **A6H8**, respectively (Figure 2, Supporting Information Computational Section, and Figure S9). Each model was solvated in a TIP3P water box with counter ions to neutralize the system. Then, independent simulations ran for

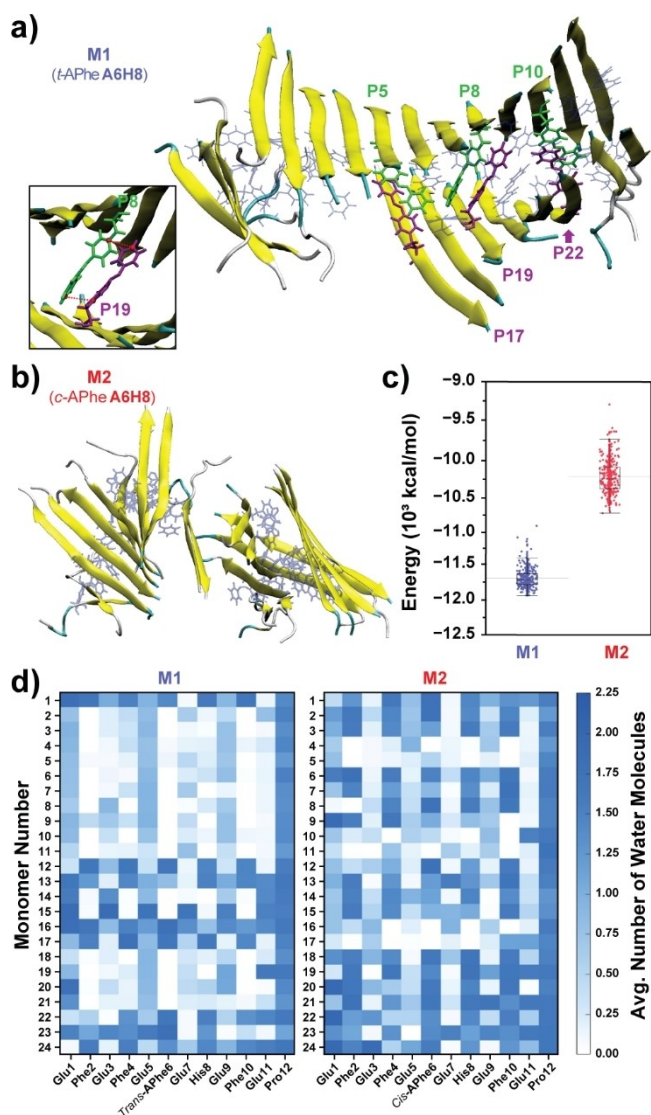


Figure 2. (a) Final simulated structure of the **M1** model, representing the *trans*-APhe **A6H8** peptide fibrils. Most of the *t*-APhe groups are shown in pale blue, while selected couples of *t*-APhe groups are highlighted in purple/green to mark the inter-sheet π - π interactions. Other side chain residues were omitted for clarity. *Insert*: higher magnification of two *t*-APhe residues, highlighting the interlayer interactions (from monomers 8 and 19); red lines mark the distances between carbon atoms that were followed along the simulation to estimate the persistence of the interactions, as presented in Figure S13. (b) Final simulated structure of the **M2** model, representing the *cis*-APhe **A6H8** peptide assemblies. MD simulations of **M1** and **M2** were repeated more times (Figure S9) and showed very similar results to the data in (a) and (b). (c) GBMV-based conformational energies of **M1** and **M2**. (d) Average number of water molecules around each amino acid in the sequence of each monomer along the fibril of **M1** and **M2**, as calculated for the last 10 ns of the simulation. In all cases, layer 1 consisted of monomers 1–12 and layer 2 consisted of monomers 13–24. For more simulation details see Supporting Information Computational Section.

each model for 100 ns at 310 K, using the NPT ensemble, as detailed in the Supporting Information section 2.^[18] The **M1** model predominantly acquired a fibrillar twisted structure

(Figure 2a, Scheme S3 and Table S1)—note that such a twist was also observed in TEM images of the *t*-APhe **A6H8** (Figure S11) and analogous previously studied peptide^[12b] fibrils—whereas the **M2** model exhibited structural defects even at the monomeric level (Figure 2b). Both models showed a convergence trend in the root-mean square deviation (RMSD) analysis (Figure S12), indicating that the simulation timescale was reasonable, and **M1** exhibited a significantly lower conformational energy compared to **M2** (Figure 2c). The structural integrity of the **M1** model was further evidenced by the formation of hydrophobic and π - π interactions between the *t*-APhe residues (*insert* to Figure 2a), which formed immediately and remained conserved throughout the entire simulation time (Figure S13). Based on the solvation analysis of the water molecules around each amino acid of the peptide monomers, considerable hydrophobicity was observed between the layers of **M1**, whereas the **M2** model allowed many more water molecules to enter the inter-sheet regions (Figure 2d). In further characterization of the final simulated structures, we found that the distances between monomers (for each sheet) and the inter-sheet distances within **M1** were significantly smaller than those within **M2** (Tables S1 and S2). Taking together all the analyzed structural features, we conclude that maintaining the intact β -sheet bilayer via formation of inter-sheet aromatic interactions makes the *t*-APhe **A6H8** fibrils significantly more stable than fibrils formed by *c*-APhe **A6H8**, leading to conversion of the latter into amorphous aggregates.

Selecting the Most Efficient Photo-Switchable Catalyst

Following the characterization of the photo-switched self-assembly process, we explored the effect of illumination and concomitant APhe isomerization on the hydrolytic activity of the His-containing peptides **H1A6**, **H5A6**, **A6H8** and **A6H12** (Figure 3 and Supporting Information Experimental methods). The catalytic capacity was evaluated by monitoring the rate of hydrolysis of the classical substrate 4-nitrophenyl acetate (*p*-NPA) in the presence of the studied catalyst, $v_i(\text{cat})$, in comparison to the rate of the background catalyst-free hydrolysis, $v_i(\text{BG})$ (Figure 3a and Figure S15). All four peptides, possessing either the *t*-APhe or *c*-APhe residues, catalysed the reaction, namely induced faster than background hydrolysis, and they were found to be more active than the control **A6** and base peptides that lack the His residue (Figure 3a). Certain histidine positions along the sequence were found to be more efficient than others for enhancing activity, as well as for emphasizing the activity difference between the (*t*-APhe) fibrillar versus (*c*-APhe) unassembled peptides. The most active peptides contained a His residue on the same face as the APhe moiety, namely, at the hydrophobic face also containing the Phe residues, as can be seen by >20 times rate enhancement for **A6H8** and **A6H12** versus background (Figure 3a). The most significant difference between the hydrolysis rates in the dark and after illumination was observed for peptide **A6H8** for which the *t*-APhe isomer was twice as active as the *c*-APhe isomer

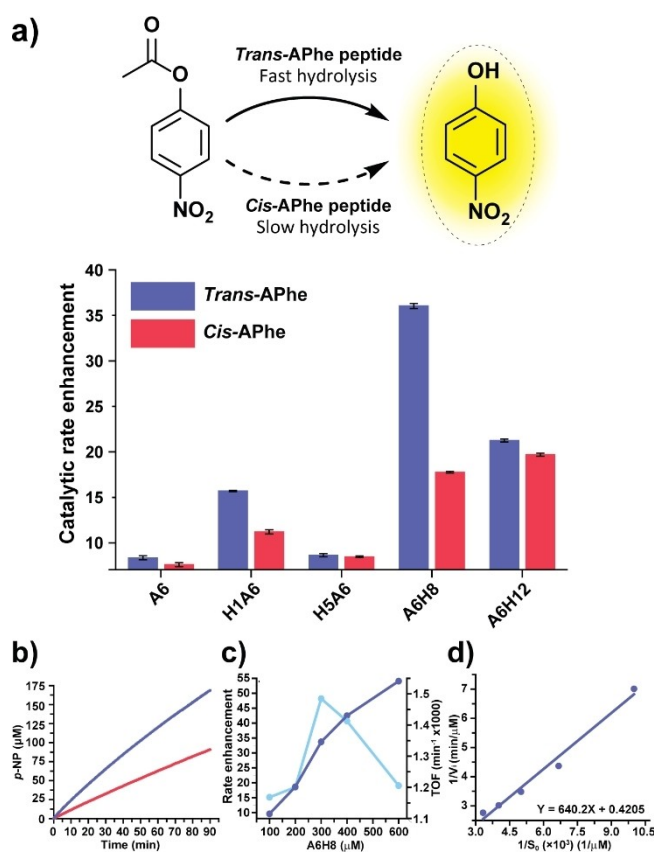


Figure 3. Light-dependent esterase activity of the A6-derived peptides. (a) Rate enhancement of (240 μM) *p*-NPA hydrolysis by all peptides (300 μM) containing the *trans*-APhe and *cis*-APhe residues. Bars showing the initial rate of the catalytic reaction divided by the initial rate of the catalyst-free hydrolysis ($v_i(\text{cat})/v_i(\text{BG})$). The Y-axis threshold is taken at rate enhancement = 7.57 as calculated for hydrolysis by the base peptide. (b) *p*-nitrophenol (*p*-NP) concentrations as a function of time for reactions catalysed by *t*-APhe **A6H8** and *c*-APhe **A6H8**; net activity is shown after subtracting *p*-NP amounts formed in the catalyst-free hydrolysis. (c) Rate enhancement of (240 μM) *p*-NPA hydrolysis with different concentrations of *t*-APhe **A6H8** (dark blue curve), and the respective turnover frequencies obtained by dividing the net rate in the presence of catalyst ($\mu\text{M}/\text{min}$) by the catalyst (μM) amount (light blue). (d) Lineweaver–Burk plot calculated from the initial hydrolysis rates of variable *p*-NPA substrate concentrations (100–300 μM) by (300 μM) *t*-APhe **A6H8**. Raw kinetic data is given in Figure S15. All experiments were carried out in 50 mM phosphate buffer pH 6.0 at 25 °C.

(Figure 3b). This result perfectly correlates with the large difference in assembly morphology observed above for *t*-APhe **A6H8** and *c*-APhe **A6H8** (Figures 1 and 2), again supporting the selection of **A6H8** as the most useful photo-switchable peptide in our library.

Analysis of the *p*-NPA hydrolysis by different concentrations of *t*-APhe **A6H8** (100–600 μM) revealed a monotonic increase in rate with elevated concentrations (Figure 3c). The turnover frequency (TOF) values extracted from this assay showed an optimal efficiency for hydrolysis at 300 μM peptide (Figure 3c; light blue), and accordingly this concentration was used for the following studies. The Michaelis–Menten constants for the esterase-like kinetics were de-

duced from the double-reciprocal plot of the initial rates versus substrate concentrations (Figure 3d): K_M was found to be 1.52 ± 0.15 mM, the rate constant $k_{\text{cat}} = 1.32 \pm 0.16 \cdot 10^{-4} \text{ s}^{-1}$, and the catalytic efficiency (k_{cat}/K_M) $0.086 \pm 0.03 \text{ M}^{-1} \cdot \text{s}^{-1}$. While, as expected, the ester hydrolysis by **A6H8** was less efficient than that observed for natural esterase enzymes or metallopeptides,^[19] the current k_{cat}/K_M value is comparable to previous reports of catalysis by His-containing β -sheet fibres, and related supramolecular organocatalysts.^[15c,20] We noted that hydrolysis by *c*-APhe **A6H8** did not follow Michaelis–Menten kinetics.

Alternating Control Over the Self-Assembly and Catalytic Activity by Light

We next explored the possibility of reversibly switch the assembly morphology and catalytic activity of **A6H8** by alternate illumination with UV light for *trans*-to-*cis* isomerization, and visible light for the reverse *cis*-to-*trans* isomerization (Scheme 1a and Figure 4). Azobenzene typically presents high stability against photobleaching.^[15d] To confirm the durability of the APhe group when attached to the **A6H8** sequence, five photoisomerization cycles were performed, during which reasonable reversibility was found with little fatigue, and a recovery ratio $\geq 91\%$ for each cycle (Figure 4a and Figure S4e). The self-assembly switch was characterized using the ThT staining assay (Figure 4b), AFM (Figure 4c), and TEM (Figure 4d). For the microscopy studies, a stock solution of **A6H8** at pH 6.0 was prepared and alternately exposed to the UV and Vis irradiation (30 min each). A defined amount was withdrawn from this solution after each illumination step, diluted in buffer to get the final 200 μM peptide concentration, and subsequently drop-cast on a mica/grid surface to record the AFM or TEM images (Experimental section, SI). It can be clearly seen from these assays that fibrillar aggregates were obtained for the *t*-APhe **A6H8**; such fibrils were absent (or minimally retained) after UV irradiation and isomerization to *c*-APhe **A6H8**, and then regenerated following irradiation with visible light, albeit reflecting nominal structure degradation due probably to the incomplete APhe residue isomerization (Figure 4a).

The catalytic activity switch of **A6H8** was also investigated under alternating illumination conditions, affecting multiple assembly-disassembly cycles, in-turn significantly enhancing (on) or halting (off) *p*-NPA hydrolysis (Figure 4e). The experiments were performed in a similar way to the assembly switch, by exposing the **A6H8** stock solutions to UV and Vis irradiation cycles (30 min each step), while removing aliquots after each step. These aliquots were diluted into the buffer solution, reaching 300 μM peptide and 200 μM *p*-NPA concentrations, and the catalytic activity was monitored. The activity could be reasonably switched to the expected levels during the first three cycles, while some fatigue was observed for the 4th and 5th cycles, after which the experiment ended. The fatigue may result from the partial bleaching of the azobenzene groups (panel a) and

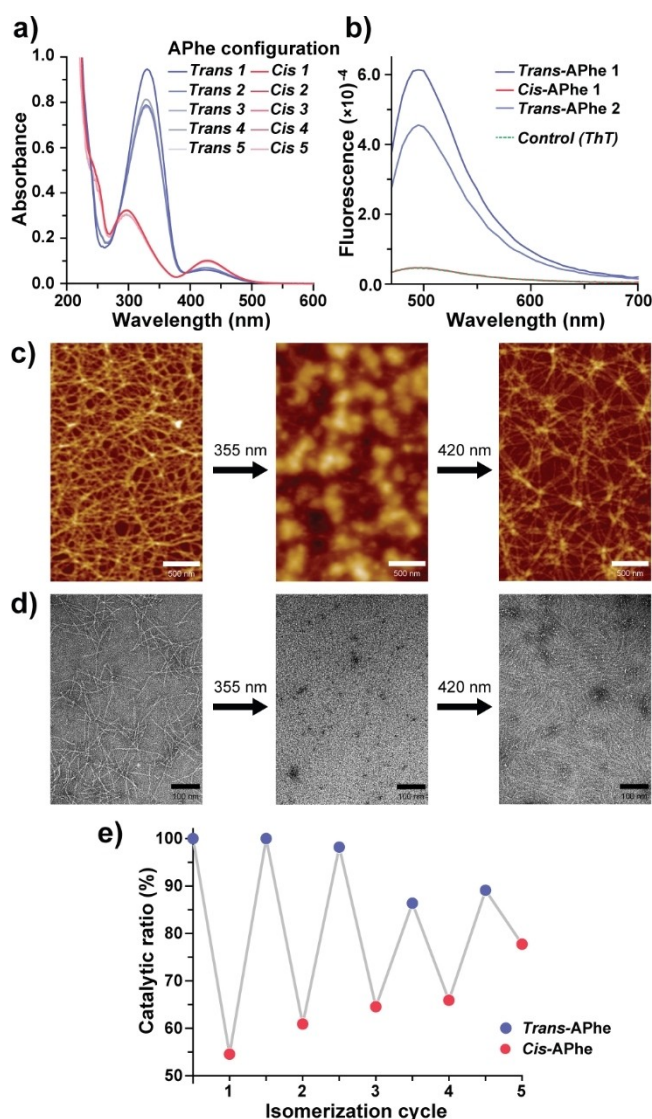


Figure 4. Continuous switching of **A6H8** assembly and catalytic activity. (a) UV/Vis spectra measured over five illumination cycles for **A6H8** solutions after UV light illumination (355 nm) for *trans*-to-*cis* APhe isomerization and visible light illumination (420 nm) for the reverse *cis*-to-*trans* APhe isomerization. (b) Fluorescence emission spectra obtained for (200 μM) **A6H8** staining by (100 μM) ThT in a complete photoisomerization cycle. Control results show the background ThT emission. (c) AFM and (d) TEM images of (200 μM) **A6H8** assemblies obtained in a complete photoisomerization cycle. (e) Catalytic rate of *p*-NPA hydrolysis by **A6H8** over five APhe isomerization cycles. The net hydrolysis rate by *t*-APhe **A6H8** at initiation was taken as 100% activity. All experiments were carried out in 50 mM phosphate buffer pH 6.0 at 25 °C.

some irreversibility in the assembly process, as seen in panels (c) and (d).

Enantioselective Hydrolysis by the Photo-Switchable Catalyst

Similar to hydrolysis by other peptide fibril catalysts, **A6H8** activity is affected by substrate recognition at the fibre

vicinity and the increased basicity of His residues that are hydrogen-bonded to nearby functional groups (including adjacent His groups).^[21] Unlike the active sites of globular enzymes that induce regioselective and stereoselective catalysis, except for rare cases, the peptide fibres shallow interaction interfaces could not support (or have not been assayed for) stereoselective substrate recognition and enantioselective reactions. Yet, since only all *L*-amino acid peptides were employed here for forming the fibrils, we postulated that enantioselectivity (even if modest) could be achieved (Figure 5) and furthermore modulated by light.

To explore the enantioselectivity by **A6H8**, the hydrolysis rate enhancement was assayed towards the chiral ester substrates 4-nitrophenyl-(*tert*-butoxycarbonyl)-*L/D*-alaninate, named Boc-*L*-Ala-ONp and Boc-*D*-Ala-ONp (Figure 5). Indeed, even for these non-bulky chiral substrates, *t*-APhe **A6H8** was found to be significantly more active for the hydrolysis of one enantiomer, Boc-*L*-Ala-ONp, versus the other, Boc-*D*-Ala-ONp. Figure 5b, and the reactivity profile for the hydrolysis of Boc-*L/D*-Ala-ONp mixtures at different ratios by *t*-APhe **A6H8** (Figure S20b), reveal more than 4-fold initial rate difference towards the *L*-substrate, equivalent to >60% enantiomeric excess in the hydrolysis of racemic mixtures. This performance is comparable to that of the best chiroselective fibril esterases previously reported in aqueous mixtures.^[4a,b] The kinetic constants determined for the hydrolysis of Boc-*L*-Ala-ONp using the double-reciprocal plot of the initial rates versus variable substrate concentrations are: $K_M = 1.23 \pm 0.11$ mM, $k_{cat} = 2.90 \pm 0.2 \cdot 10^{-4}$ s⁻¹, $k_{cat}/K_M = 0.235 \pm 0.013$ M⁻¹·s⁻¹ (Figure 5c).

By studying the effect of alternate illumination on the enantioselective system we revealed similar behaviour to that observed for the *p*-NPA catalytic switch. The *trans*-to-*cis* APhe isomerization by UV light led to a significant reduction in activity towards both the *L*-Ala (*blue/red* bars in Figure 5d) and *D*-Ala (*light blue/pink* bars) substrates, and furthermore, the activity was perfectly restored after APhe *cis*-to-*trans* isomerization by visible light (Figure 5d and Figure S22). This result point to a potentially interesting prebiotic mechanism, by which one compound in a racemic mixture (e.g. the *L*-amino acid), is formed through catalysis by the *trans*-azobenzene isomer and selected over a competitor molecule that, following catalyst irradiation, is formed much more slowly by the *cis*-isomer.

Conclusions

This study describes reversible control over several cycles of peptide esterase activity. Light triggering is used for temporal, on-demand stimulation of an interesting mechanistic sequence, where the *trans/cis* molecular isomerization leads to changes in the peptide self-assembly state, which in turn controls the catalytic activity. This demonstration might be relevant for scenarios that facilitated the emergence of function in the prebiotic environment, and for the development of new devices for bio-nanotechnology.

It is already accepted that spontaneous oligomerization of short peptides could take place during early chemical

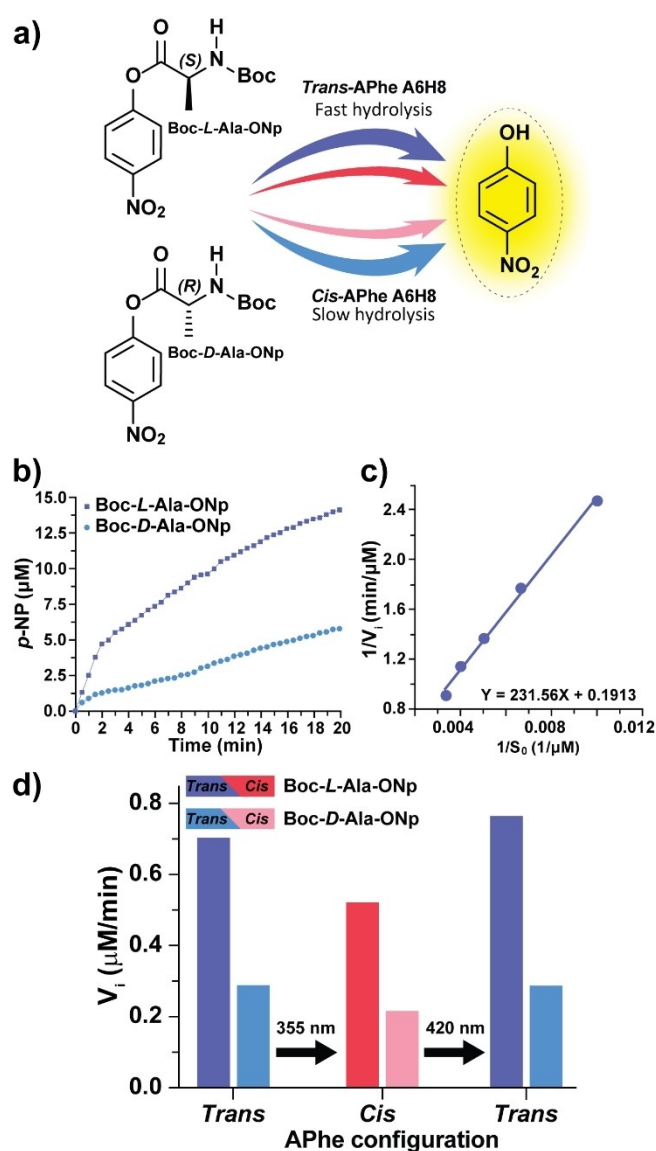


Figure 5. Enantioselective hydrolysis by **A6H8**. (a) Schematic description of the hydrolysis of Boc-*L*-Ala-ONp and Boc-*D*-Ala-ONp substrates in the presence of the strong and weak catalysts, *t*-APhe **A6H8** and *c*-APhe **A6H8**, respectively. (b) Net formation of *p*-NP over time in reactions of the enantiomeric substrates (200 μM) in the presence of 300 μM *t*-APhe **A6H8**. (c) Lineweaver–Burk plot calculated for hydrolytic reactions of 300 μM *t*-APhe **A6H8** with variable Boc-*L*-Ala-ONp concentrations (100–300 μM). (d) Initial rate of (net) *p*-NP formation during hydrolysis of Boc-*L*-Ala-ONp and Boc-*D*-Ala-ONp, alternately catalyzed by *t*-APhe **A6H8**, *c*-APhe **A6H8**, and again *t*-APhe **A6H8**. Reactions were performed in 50 mM phosphate buffer pH 6.5 at 25 °C. The synthesis of Boc-*L*-Ala-ONp and Boc-*D*-Ala-ONp from the amino acid precursors and their characterizations are described in Figures S17–S19, and Scheme S2, and the raw kinetic data is shown in Figures S20–S22.

evolution by various routes of (carboxylic acid) monomer activation, and furthermore that amphiphilic sequences which were formed in the prebiotic soup could interact with each other and assemble in aqueous environments.^[1c,10] Now, after several groups, including our team, have shown that aggregation of the prebiotic peptides into supramolecular

architectures such as spheres, fibres and nanotubes, can induce their catalytic activity, we confirmed that an additional minor modification, namely the replacement ('mutation') of a Phe residue for APhe, is sufficient for the emergence of new regulatory machinery, potentially propelled by sunlight on the early Earth.

Recent advances in the development of supramolecular peptide assemblies revealed their utility in various applications beyond catalysis, such as electroactive, coatings, and gel phase materials. The design of these materials is flexible and typically cost effective, and the products are biocompatible and ecologically friendly. We propose that incorporating light-driven functionality into molecules driving such devices may expand their appeal for potential industrial in the near future.

Acknowledgements

GA acknowledges project funding from NSF-BSF (BSF 2019745) and Horizon Europe ERC synergy (MiniLife; No. 101118938). DW acknowledges the financial support of Leiden University and China Scholarship Council (CSC) (No. 20200831017). We thank B. Pramanik for helping with the microscopy studies, and the support of the BGU HPC computational center staff.

Conflict of Interest

The authors declare no conflict of interest.

Data Availability Statement

The data that support the findings of this study are available on request from the corresponding author. The data are not publicly available due to privacy or ethical restrictions.

Keywords: Systems Chemistry · Light triggering · Peptide catalysis · Dynamic self-assembly · Stereoselective catalysis

- [1] a) C. P. J. Maury, *Cell. Mol. Life Sci.* **2018**, *75*, 1499–1507; b) D. Kroiss, G. Ashkenasy, A. B. Braunschweig, T. Tuttle, R. V. Ulijn, *Chem* **2019**, *5*, 1917–1920; c) Y. Bai, A. Chotera, O. Taran, C. Liang, G. Ashkenasy, D. G. Lynn, *Chem. Soc. Rev.* **2018**, *47*, 5444–5456; d) P. Adamski, M. Elefeld, A. Sood, Á. Kun, A. Szilágyi, T. Czárán, E. Szathmáry, S. Otto, *Nat. Chem. Rev.* **2020**, *4*, 386–403; e) J. Sola, C. Jimeno, I. Alfonso, *Chem. Commun.* **2020**, *56*, 13273–13286; f) N. Nogal, M. Sanz-Sánchez, S. Vela-Gallego, K. Ruiz-Mirazo, A. de la Escosura, *Chem. Soc. Rev.* **2023**, *52*, 7359–7388.
- [2] a) N. Singh, M. Kumar, J. F. Miravet, R. V. Ulijn, B. Escuder, *Chem. Eur. J.* **2017**, *981–993*; b) O. Zozulia, M. A. Dolan, I. V. Korendovych, *Chem. Soc. Rev.* **2018**, *47*, 3621–3639; c) A. Chatterjee, A. Reja, S. Pal, D. Das, *Chem. Soc. Rev.* **2022**, *51*, 3047–3070; d) M. Amit, S. Yuran, E. Gazit, M. Reches, N. Ashkenasy, *Adv. Mater.* **2018**, *30*, 1707083; e) Y. Gao, F. Zhao, Q.-G. Wang, Y. Zhang, B. Xu, *Chem. Soc. Rev.* **2010**, *39*, 3425–3433; f) Y. Zhang, X. Tian, X. Li, *Journal of Materials Chemistry B: Materials for Biology and Medicine* **2022**, *10*, 3716–3722; g) J. Chen, K. Shi, R. Chen, Z. Zhai, P. Song, L. W. Chow, R. Chandrawati, E. T. Pashuck, F. Jiao, Y. Lin, *Angew. Chem. Int. Ed.* **2024**, *63*, e202317887; h) N. Singh, M. Tena-Solsona, J. F. Miravet, B. Escuder, *Isr. J. Chem.* **2015**, *55*, 711–723.
- [3] a) C. M. Rufo, Y. S. Moroz, O. V. Moroz, J. Stoehr, T. A. Smith, X. Hu, W. F. DeGrado, I. V. Korendovych, *Nat. Chem.* **2014**, *6*, 303–309; b) O. Zozulia, L. R. Marshall, I. Kim, E. M. Kohn, I. V. Korendovych, *Chem. Eur. J.* **2021**, *27*, 5388–5392.
- [4] a) Y. S. Moroz, T. T. Dunston, O. V. Makhlynets, O. V. Moroz, Y. Wu, J. H. Yoon, A. B. Olsen, J. M. McLaughlin, K. L. Mack, P. M. Gosavi, N. A. J. van Nuland, I. V. Korendovych, *J. Am. Chem. Soc.* **2015**, *137*, 14905–14911; b) A. Singh, S. Goswami, P. Singh, D. Das, *Angew. Chem. Int. Ed.* **2023**, *62*, e202315716; c) J. L. Heier, D. J. Mikolajczak, C. Böttcher, B. Kopsch, *Biopolymers* **2017**, *108*; d) Z. Li, S. Y. Joshi, Y. Wang, S. A. Deshmukh, J. B. Matson, *Angew. Chem. Int. Ed.* **2023**, *62*, e202303755.
- [5] C. Zhang, R. Shafi, A. Lampel, D. MacPherson, C. G. Pappas, V. Narang, T. Wang, C. Maldarelli, R. V. Ulijn, *Angew. Chem. Int. Ed.* **2017**, *56*, 14511–14515.
- [6] Q. Li, J. Min, J. Zhang, M. Reches, Y. Shen, R. Su, Y. Wang, W. Qi, *Angew. Chem. Int. Ed.* **2023**, *62*, e202309830.
- [7] a) P. Gorostiza, E. Y. Isacoff, *Science* **2008**, *322*, 395–399; b) W. A. Velema, J. P. van der Berg, M. J. Hansen, W. Szymanski, A. J. M. Driessen, B. L. Feringa, *Nat. Chem.* **2013**, *5*, 924–928.
- [8] a) S. Neri, S. Garcia Martin, C. Pezzato, L. J. Prins, *J. Am. Chem. Soc.* **2017**, *139*, 1794–1797; b) N. Ma, F. Li, S. Li, S. Chu, L. Han, S. Liu, T. Yan, R. Tian, Q. Luo, J. Liu, *Nanoscale* **2019**, *11*, 3521–3526; c) C. Z.-J. Ren, P. Solís Muñana, J. Dupont, S. S. Zhou, J. L.-Y. Chen, *Angew. Chem. Int. Ed.* **2019**, *58*, 15254–15258; d) X. Xie, L. Wang, X. Liu, Z. Du, Y. Li, B. Li, L. Wu, W. Li, *Chem. Commun.* **2020**, *56*, 1867–1870; e) K. Liu, A. Blokhuis, C. van Ewijk, A. Kiani, J. Wu, W. H. Roos, S. Otto, *Nat. Chem.* **2024**, *16*, 79–88.
- [9] S. Goswami, A. Reja, S. Pal, A. Singh, D. Das, *J. Am. Chem. Soc.* **2022**, *144*, 19248–19252.
- [10] M. Frenkel-Pinter, M. Samanta, G. Ashkenasy, L. J. Leman, *Chem. Rev.* **2020**, *11*, 4707–4765.
- [11] a) H. Rapaport, *Supramol. Chem.* **2006**, *18*, 445–454; b) H. Rapaport, K. Kjaer, T. R. Jensen, L. Leiserowitz, D. A. Tirrell, *J. Am. Chem. Soc.* **2000**, *122*, 12523–12529; c) Y. Raz, B. Rubinov, M. Matmor, H. Rapaport, G. Ashkenasy, Y. Miller, *Chem. Commun.* **2013**, *49*, 6561–6563; d) B. Rubinov, N. Wagner, H. Rapaport, G. Ashkenasy, *Angew. Chem. Int. Ed.* **2009**, *48*, 6683–6686.
- [12] a) D. Ivnikski, M. Amit, B. Rubinov, R. Cohen-Luria, N. Ashkenasy, G. Ashkenasy, *Chem. Commun.* **2014**, *50*, 6733–6736; b) D. Ivnikski, M. Amit, O. Silberbush, Y. Atsmon-Raz, J. Nanda, R. Cohen-Luria, Y. Miller, G. Ashkenasy, N. Ashkenasy, *Angew. Chem. Int. Ed.* **2016**, *55*, 9988–9992.
- [13] M. Tena-Solsona, J. Nanda, S. Diaz-Oltra, A. Chotera, G. Ashkenasy, B. Escuder, *Chem. Eur. J.* **2016**, *22*, 6687–6694.
- [14] a) B. Rubinov, N. Wagner, M. Matmor, O. Regev, N. Ashkenasy, G. Ashkenasy, *ACS Nano* **2012**, *6*, 7893–7901; b) J. Nanda, B. Rubinov, D. Ivnikski, R. Mukherjee, E. Shtelman, Y. Motro, Y. Miller, N. Wagner, R. Cohen-Luria, G. Ashkenasy, *Nat. Commun.* **2017**, *8*, 434.
- [15] a) A. A. Beharry, G. A. Woolley, *Chem. Soc. Rev.* **2011**, *40*, 4422–4437; b) R. J. Mart, R. K. Allemann, *Chem. Commun.* **2016**, *52*, 12262–12277; c) Y. Zhao, B. Lei, M. Wang, S. Wu, W. Qi, R. Su, Z. He, *Journal of Materials Chemistry B: Materials for Biology and Medicine* **2018**, *6*, 2444–2449; d) C. Renner, L. Moroder, *ChemBioChem* **2006**, *7*, 868–878.

- [16] N. S. A. Crone, N. van Hilten, A. van der Ham, H. J. Risselada, A. Kros, A. L. Boyle, *Bioconjugate Chem.* **2023**, *34*, 345–357.
- [17] a) R. Song, X. Wu, B. Xue, Y. Yang, W. Huang, G. Zeng, J. Wang, W. Li, Y. Cao, W. Wang, J. Lu, H. Dong, *J. Am. Chem. Soc.* **2019**, *141*, 223–231; b) C. Ghosh, S. Menon, S. Bal, S. Goswami, J. Mondal, D. Das, *Nano Lett.* **2023**, *23*, 5828–5835.
- [18] D. M. Heyes, *Chem. Phys.* **1983**, *82*, 285–301.
- [19] a) Z. S. Al-Garawi, B. A. McIntosh, D. Neill-Hall, A. A. Hatimy, S. M. Sweet, M. C. Bagley, L. C. Serpell, *Nanoscale* **2017**, *9*, 10773–10783; b) J. A. Verpoorte, S. Mehta, J. T. Edsall, *J. Biol. Chem.* **1967**, *242*, 4221–4229.
- [20] a) C. Zhang, X. Xue, Q. Luo, Y. Li, K. Yang, X. Zhuang, Y. Jiang, J. Zhang, J. Liu, G. Zou, X.-J. Liang, *ACS Nano* **2014**, *8*, 11715–11723; b) A. J. Nicoll, R. K. Allemann, *Org. Biomol. Chem.* **2004**, *2*, 2175–2180; c) D. J. Mikolajczak, J. L. Heier, B. Schade, B. Kocsch, *Biomacromolecules* **2017**, *18*, 3557–3562; d) I. W. Hamley, *Biomacromolecules* **2021**, *22*, 1835–1855.
- [21] a) K. S. Broo, H. Nilsson, J. Nilsson, L. Baltzer, *J. Am. Chem. Soc.* **1998**, *120*, 10287–10295; b) P. Makam, S. S. R. K. C. Yamijala, K. Tao, L. J. W. Shimon, D. S. Eisenberg, M. R. Sawaya, B. M. Wong, E. Gazit, *Nat. Cat.* **2019**, *2*, 977–985.

Manuscript received: July 22, 2024

Accepted manuscript online: September 27, 2024

Version of record online: November 6, 2024